AGU PUBLICATIONS

JGR

Journal of Geophysical Research: Space Physics

RESEARCH ARTICLE
10.1002/2017JA024197

Key Points:
- Strong transverse and field-aligned currents within sub-ion magnetic holes
- These magnetic hole structures are sustained by electron diamagnetic and Hall currents
- Modulation of ECH wave intensity by sub-ion magnetic holes

Correspondence to:
X.-J. Zhang,
xjzhang@ucla.edu

Citation:
Zhang, X.-J., A. Artemyev, V. Angelopoulos, and R. B. Horne (2017), Kinetics of sub-ion scale magnetic holes in the near-Earth plasma sheet, *J. Geophys. Res. Space Physics*, *122*, 10,304–10,317, doi:10.1002/2017JA024197.

Received 28 MAR 2017
Accepted 3 AUG 2017
Accepted article online 7 AUG 2017
Published online 21 OCT 2017

Kinetics of sub-ion scale magnetic holes in the near-Earth plasma sheet

X.-J. Zhang[1,2], A. Artemyev[1,3], V. Angelopoulos[1], and R. B. Horne[4]

[1]Department of Earth, Planetary, and Space Sciences, University of California, Los Angeles, California, USA, [2]Department of Atmospheric and Oceanic Sciences, University of California, Los Angeles, California, USA, [3]Space Research Institute, Russian Academy of Sciences, Moscow, Russia, [4]British Antarctic Survey, Natural Environment Research Council, Cambridge, UK

Abstract In collisionless space plasmas, the energy cascade from larger to smaller scales requires effective interactions between ions and electrons. These interactions are organized by sub-ion scale plasma structures in which strong electric fields connect demagnetized ions to magnetized electrons. We consider one such structure, magnetic holes, observed by THEMIS spacecraft in the dipolarized hot plasma sheet. Magnetic holes are localized depressions of the magnetic field with strong currents at their boundaries. Taking advantage of slow plasma convection (~10–20 km/s), we reconstruct the electron velocity distribution within magnetic holes and demonstrate that the current at their boundaries is predominantly carried by magnetized thermal electrons. The motion of these electrons is the combination of diamagnetic drift and $\mathbf{E} \times \mathbf{B}$ drift in a Hall electric field. Magnetic holes can effectively modulate the intensity of electron cyclotron harmonic waves, and thus the spatial distribution of thermal electron precipitation. They may also contain field-aligned currents with magnitudes of ~5 nA/m^2 (1 order of magnitude smaller than the cross-field current density). Therefore, sub-ion scale magnetic holes can be important for ionosphere-magnetosphere coupling.

1. Introduction

Electromagnetic and plasma energies in the hot magnetotail plasma are distributed in structures with a wide range of spatial scales: from MHD wave scales, ~10^4 km [e.g., *Zhang et al.*, 2005; *Runov et al.*, 2009a], to ion scales, ~100–1000 km (e.g., current sheets, dipolarization fronts, and kinetic Alfven waves [*Petrukovich et al.*, 2015; *Runov et al.*, 2009b; *Chaston et al.*, 2012]), and to electron scales, ~0.1–10 km (e.g., whistler mode or cyclotron waves [e.g., *Le Contel et al.*, 2009; *Deng et al.*, 2010; *Zhang et al.*, 2014] and electrostatic solitons [e.g., *Matsumoto et al.*, 1994; *Khotyaintsev et al.*, 2010]). Corresponding timescales vary from millihertz range to kilohertz range (see *Bauer et al.* [1995], *Huang et al.* [2012], *Vörös* [2011], *Zelenyi et al.* [2015], and references therein for discussions about the contribution of various plasma waves/structures to different frequency ranges).

Sub-ion scale (from ion gyroradius ρ_i to electron scale) structures play an important role in the entire electromagnetic energy spectrum. In this hybrid (or sub-ion) range are various plasma structures with electromagnetic field gradients strong enough to decouple ions (which are not responsive to $\mathbf{E} \times \mathbf{B}$ drift because of their large gyroradii) from magnetized electrons. Hall effects (e.g., strong electric fields and field-aligned currents) are known to exist within such plasma structures (see examples in *Wygant et al.* [2005], *Teh et al.* [2011], *Fu et al.* [2012], and *Norgren et al.* [2012]). Spatial and temporal scales of sub-ion plasma structures enable effective energy exchange between the thermal ion population (containing most of the plasma energy in the magnetotail due to small electron temperature and weak plasma flows [see, e.g., *Hoshino et al.*, 2000; *Artemyev et al.*, 2011; *Wang et al.*, 2012]) and the electron population (responsible for transporting energy to the aurora region via precipitations and field-aligned currents [see *Thorne et al.*, 2010; *Lysak and Song*, 2011; *Ni et al.*, 2016]). Well-known sub-ion structures include very thin current sheets [e.g., *Nakamura et al.*, 2006; *Artemyev et al.*, 2013], small-scale plasmoids [*Teh et al.*, 2010; *Wang et al.*, 2016], and intense dipolarization fronts [e.g., *Sergeev et al.*, 2009; *Hwang et al.*, 2011; *Angelopoulos et al.*, 2013]. Because they are extremely dynamical (transient) structures with significant electromagnetic fluctuations, investigations of their kinetics (e.g., particle distributions and relation to wave activity) are largely constrained by the resolution of spacecraft measurements.

Recent spacecraft observations have revealed a new type of sub-ion plasma structure in the quiet-time (dipolarized) magnetotail: sub-ion magnetic holes (MHs), i.e., small-scale depressions of the background magnetic field. Spacecraft observations [e.g., *Soucek et al.*, 2008; *Ge et al.*, 2011] and theoretical models [e.g., *Kuznetsov et al.*, 2007; *Califano et al.*, 2008] suggest that such MHs represent a nonlinear stage of the mirror-mode instability driven in the postsubstorm magnetotail by a hot anisotropic ion population. However, there are also alternative interpretations of the MH: e.g, *Balikhin et al.* [2012] suggested that MHs can be formed by an oblique tearing instability, whereas *Li et al.* [2016] and *Yao et al.* [2017] proposed that MHs can be explained by the magnetosonic soliton model. Regardless of the source of MHs, they are sub-ion scale kinetic structures in which Hall effects play an important role in the current generation [*Gershman et al.*, 2016; *Goodrich et al.*, 2016b, 2016a; *Yao et al.*, 2017].

Strong magnetic field gradients at MH boundaries result in decoupling of ion and electron motion. The electric field generated by charge separation, the Hall electric field, peaks at the hole boundary [*Schindler et al.*, 2012; *Goodrich et al.*, 2016a]. In a cylindrical geometry, such electrostatic fields drive electron vortexes centered in the hole's symmetry axis [*Roytershteyn et al.*, 2015; *Haynes et al.*, 2015], supporting electric currents at its boundary [*Gershman et al.*, 2016; *Goodrich et al.*, 2016a]. The corresponding electron velocity distribution is highly anisotropic [*Sun et al.*, 2012; *Sundberg et al.*, 2015; *Gershman et al.*, 2016; *Yao et al.*, 2017]. Therefore, sub-ion magnetic holes can significantly change local plasma properties responsible for excitation and damping of electron-scale waves [e.g., *Tenerani et al.*, 2013]. To investigate the kinetics of sub-ion MHs and their role in modifying electron properties in the postsubstorm magnetotail, a statistical study of well-resolved magnetic holes is needed.

In this study, we present Time History of Events and Macroscale Interactions during Substorms (THEMIS) spacecraft observations of a series of sub-ion scale MHs generated in the dipolarized magnetotail. Taking advantage of the slow MH convection measured at the time, we resolve the internal kinetic structure of these holes and study the electron population trapped within them. We demonstrate that sub-ion scale holes can significantly modify the properties of the plasma sheet electron population, resulting in modulations of electron cyclotron harmonic (ECH) waves in the magnetotail.

2. Data and Methodology

THEMIS observations are used in this study. We utilize background magnetic field data (with a cadence of 0.25 s) from the Flux-Gate Magnetometer (FGM) [*Auster et al.*, 2008], electron and ion measurements from Electrostatic Analyzer (ESA; energy range from few eV to ~25 keV) [*McFadden et al.*, 2008] and Solid State Telescope (SST; energy range from ~40 keV to ~700 keV) [*Angelopoulos*, 2008], and wave electric field spectra (mean amplitude of the electric field in six logarithmically spaced frequency bands from 0.1 Hz to 6 kHz) from Filter Bank (FBK) data [*Cully et al.*, 2008] at a cadence of 4 s. We also use spin resolution (~3 s) measurements of the DC electric field from the Electric Field Instrument (EFI) [*Bonnell et al.*, 2008].

Figure 1 shows an overview of the background magnetic field and plasma measurements during this event on 17 February 2010 (04:40–05:40 UT). The spacecraft, THEMIS D, which was located near the equatorial plane (magnetic field magnitude B is dominated by B_z; GSM coordinates used unless otherwise stated), observed slow ion convection (cross-field) motion with a velocity less than 30 km/s. The velocity v_z does not contribute to cross-field convection (because the background magnetic field is dominated by B_z). This component is small during the entire interval of this event, so we assume $v_z \sim 0$. This assumption is supported by observations of very small and almost constant B_x magnetic field, which would otherwise vary significantly in the magnetotail configuration with a finite v_z [e.g., *Sergeev et al.*, 2006]. During this interval, more than 20 magnetic holes were captured as localized magnetic field depressions (see Figure 1). In this paper, we analyze the configuration and kinetic structure of these holes. To estimate the electric current density, which supports magnetic field gradients, we reconstruct the MH geometry using minimum variance (MVA) analysis [*Sonnerup and Cahill*, 1968]. Knowing the direction of the spacecraft traversing MH boundaries, we use the averaged ion convection velocity to estimate the boundary spatial scale and corresponding currents [*Ge et al.*, 2011].

Figure 1 shows that the ion velocity is fluctuating significantly and there are no clear variations of ion characteristics across MHs (similar fluctuations and absence of systematic variations are shown in the ion temperature and density, see below). Therefore, we assume that ion velocity (as well as temperature and density) is uniform across MHs and average ion measurements even further in order to suppress the effect of fluctuations.

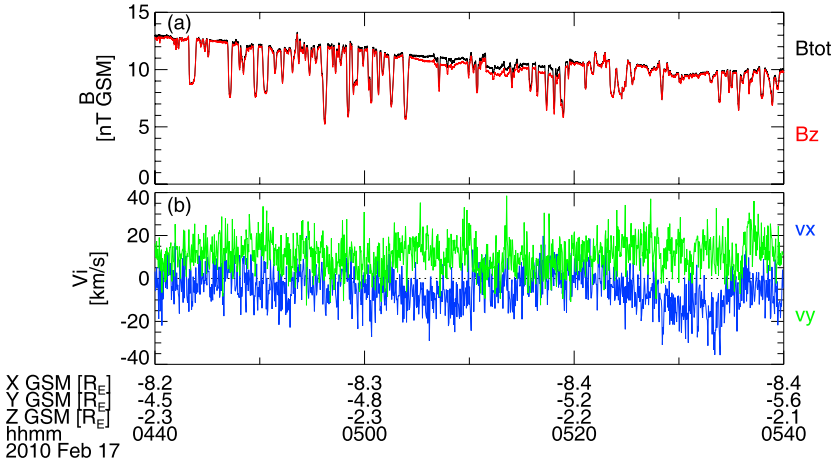

Figure 1. Overview of the event when a series of magnetic holes were captured by THEMIS D on 17 February 2010. (a) The magnetic field magnitude and the B_z component. (b) Two ion velocity components.

3. Magnetic Hole Configuration

We first investigate the general properties of MHs, pressure balance, and local geometry. Figure 2 shows details within a fragment of the interval from Figure 1, 04:50–05:05 UT. The main magnetic field component B_z is modulated by quasiperiodical MHs with amplitudes up to 50% of the background field. The ion velocity is very low, ~10–20 km/s, and thus the spatial scale of magnetic gradients at the hole boundaries is ~200–400 km (this estimate is based on the assumption that MHs convect with plasma flow, following *Ge et al.* [2011]. Fluctuations (i.e., uncertainties) in the ion temperature measurements (~5%) are stronger than the possible temperature variation across MHs. These fluctuations also mask the possible level of ion anisotropy. Therefore, we assume that the ion temperature is isotropic and does not vary across MHs, i.e., $T_{i\perp} \approx T_{i\parallel}$ ~4.6–4.8 keV. The associated ion thermal gyroradius ρ_i varies from ~600 km outside MHs to ~1800 km inside them. Therefore, we deal with sub-ion scale structures in which the spatial scale of the magnetic field gradient is smaller than ρ_i.

In the absence of ion temperature variations across MHs, the main contribution to the cross-hole pressure balance comes from plasma density and electron temperature gradients: $\Delta(B_z^2/2\mu_0) \approx k_B(T_{i\perp} + T_{e\perp})\Delta n_e + k_B n_e \Delta T_{e\perp}$ (where we assume plasma quasi-neutrality, $n_e \approx n_i$). During this event, we found rather hot electrons $T_{e\perp} \sim 3.0$–3.1 keV with $T_{i\perp}/T_{e\perp} \sim 1.5$ ($T_{i\perp}/T_{e\perp}$ in the magnetotail typically varies between 3.5 and 7 [see *Artemyev et al.*, 2011, and references therein]). The electron density (and ion density) can be obtained from ESA measurements or can be reconstructed from the spacecraft potential. However, the appreciable variation of electron temperature across MHs makes the electron density estimate from the spacecraft potential inaccurate. Therefore, in following estimates we only use the plasma density from ESA measurements, which shows almost uniform density profiles across the hole.

The characteristic magnetic field pressure drop in observed MHs is $\sim\Delta(B_z^2) \sim 25$–$75$ nT^2, whereas the contribution from the electron temperature variation is $2\mu_0 k_B n_e \Delta T_{e\perp} \sim 50$ nT^2 (we convert thermal pressure to magnetic field pressure) for $n_e \sim 0.6$ cm^{-3}, $\Delta T_{e\perp} \sim 0.1$–$0.15$ keV. Therefore, the electron temperature variation can establish the pressure balance. The density derived from ESA measurements does not vary systematically across MHs. However, due to the presence of hot ions, even a small density variation can provide some contribution to the pressure balance $2\mu_0 k_B(T_{i\perp} + T_{e\perp})\Delta n_e$. We first estimate possible effects of density and electron temperature variations on the current density generation within MHs.

With the small (sub-ion) spatial scale of these MHs, the motion of demagnetized ions is not controlled by the magnetic field, and ions can be distributed within the hole following Boltzmann's law, $n_i \sim \exp(-e\varphi/T_{i\perp})$. This is governed by the scalar potential φ generated by decoupling of ion motions from electron motions (because the electron gyroradius is less than 30 km, electrons can be assumed to be magnetized). Thus, any density variation across MHs would indicate a potential drop of $\Delta\varphi/eT_{e\perp} \sim (T_{i\perp}/T_{e\perp})\ln(1 + \Delta n_i/n_i)$, corresponding to an electric field of $\mathbf{E} = -\nabla\varphi$. If we assume that demagnetized ions do not contribute to the current density at MH boundaries, then all current $\sim\Delta B_z/200\text{km}\mu_0 \sim 15$ nA/m^2 should be carried by electrons. There are two

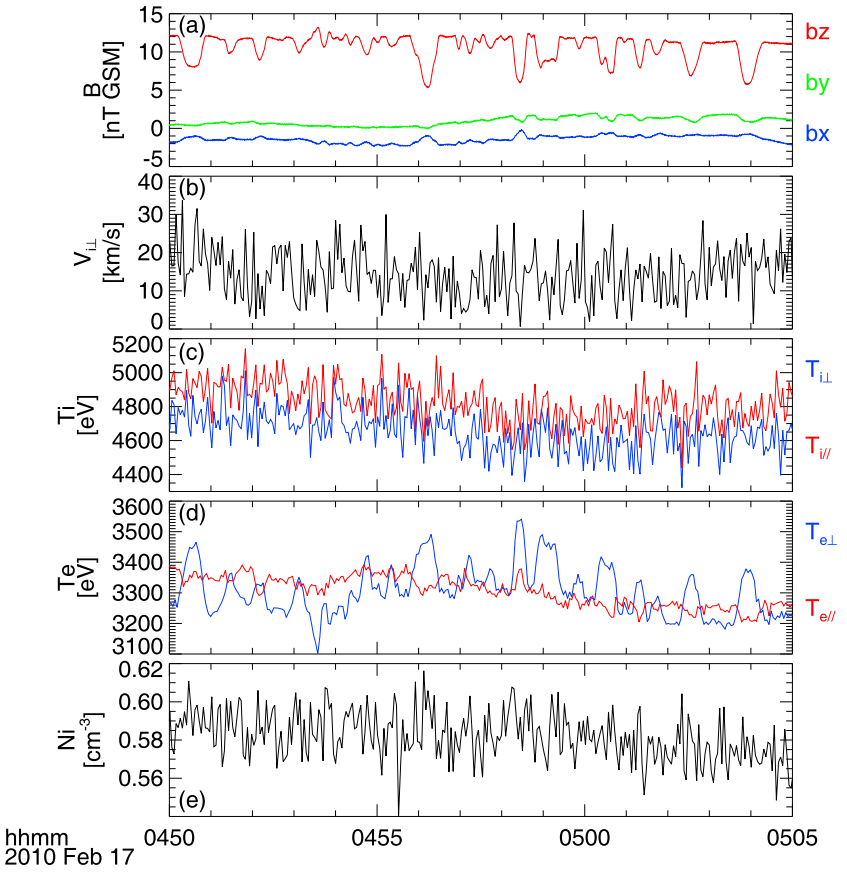

Figure 2. (a) Three magnetic field components, B_z, B_y, and B_z. (b) The ion transverse velocity, $v_i = \sqrt{v_x^2 + v_y^2}$. (c) The ion temperature, $T_{i\perp}$, $T_{i\|}$. (d) The electron temperature, $T_{e\perp}$, $T_{e\|}$. (e) The density n_i from ESA ion measurements.

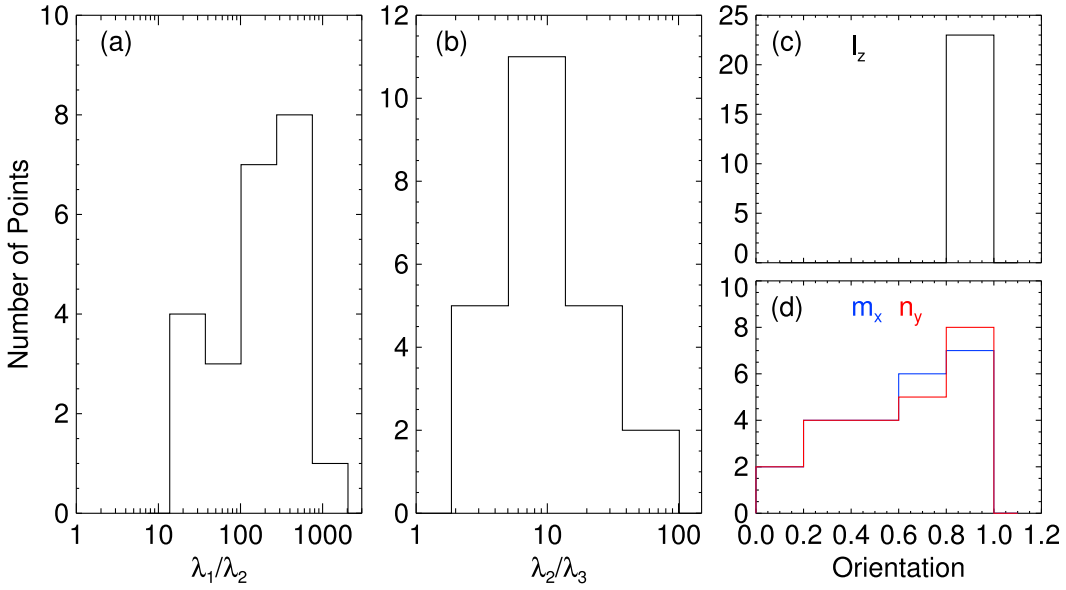

Figure 3. (a, b) Distributions of λ_1/λ_2 and λ_2/λ_3 [$\lambda_{1,2,3}$ are eigenvalues of the MVA matrix *Sonnerup and Cahill*, 1968]. (c, d) Distributions of dominant components of the MVA vectors l_z, m_x, and n_y (**l** is along the maximum variation, **n** is along the normal (minimum variation) direction, and $\mathbf{m} = \mathbf{l} \times \mathbf{n}$).

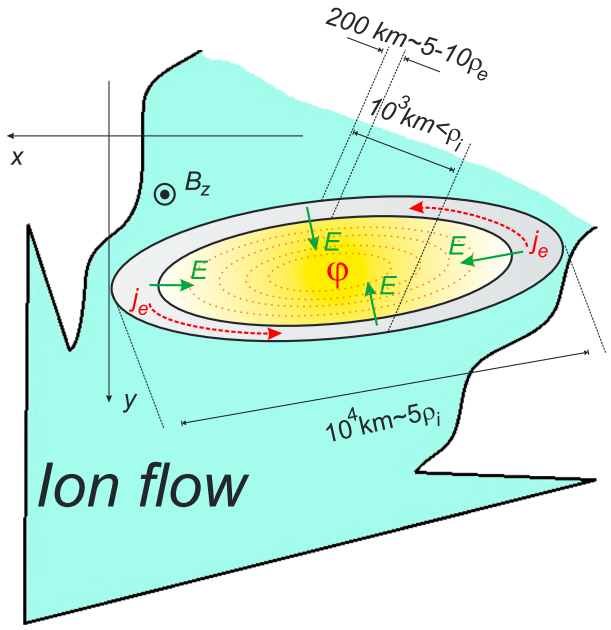

Figure 4. Scheme of magnetic hole configuration in the equatorial plane.

possible mechanisms to generate these electron currents: the electric field drift $\sim E/B_z$ [*Goodrich et al.*, 2016b, 2016a] and diamagnetic drift $\sim \nabla n_e T_e$ [*Gershman et al.*, 2016]. Measured density variations across MHs are very small, and hence the diamagnetic drift should be the dominant source for the electron current density, whereas polarization electric fields are expected to be weak. To confirm this estimate of the relative contributions of $\mathbf{E} \times \mathbf{B}$ drift and diamagnetic drift to the current density within observed MHs, we compare the estimated electric field with electric field measurements in the next section.

Balikhin et al. [2012] noted that magnetic field polarization within magnetic holes in the magnetotail is far from linear (see also multispacecraft analysis by *Sundberg et al.* [2015]). We use MVA analysis of 23 MHs to define the ratios of main (λ_1) to intermediate (λ_2) eigenvalues and intermediate (λ_2) to minimum (λ_3) eigenvalues. Figures 3a and 3b show that on average we have $\lambda_1/\lambda_2 > 100$ and $\lambda_2/\lambda_3 \leq 10$ (similar results were obtained by *Li et al.* [2016]). The main component of the **l** vector (maximum variance direction) is l_z, and the main component of the **m** vector (intermediate variance direction) is m_x. Thus, in the plane transverse to the main magnetic field component, B_z (the minimum variance direction is along y), MHs have a noncircular cross section with y scales much smaller than x scales. The n_y component of the normal vector (gradient direction) is about one for 55% of the 23 MHs, whereas n_x is about one for only 10% of the events. This indicates that the y scale of MHs is about 5 times smaller than the x scale, which is still much smaller than the inhomogeneity scale along z; i.e., MHs are in 2-D configurations, but without axial symmetry.

In the absence of multispacecraft measurements, one cannot determine how far from the MH center a spacecraft crosses the hole (see examples of 2-D hole structure reconstructed from multispacecraft observations in *Sundberg et al.* [2015] and *Gershman et al.* [2016]). Therefore, we cannot determine spatial scales between two hole boundaries. However, the dominance of MHs with $n_y \gg n_x$ and the absence of MHs with significant n_x allow us to generalize our results from Figures 2 and 3 in a schematic of the MH configuration (Figure 4). Magnetic holes are stretched in the equatorial plane with a gradient along y much stronger than that along x. Thus, currents generated by the electron cross-field drift flow predominantly along x. This drift results from pressure gradients (diamagnetic drift) and the potential drop toward the center of the hole, which is generated by the decoupling of ion and electron motions. Such a stretched configuration can be caused by strong, accelerating, earthward plasma flows in the magnetotail during the formation of holes, e.g., the observed holes could be formed within the reconnection outflow region. This scenario is also supported by the fact that ion thermal anisotropies (which can serve as the free-energy source for MHs [e.g., *Kuznetsov et al.*, 2007; *Soucek et al.*, 2008]) in the Earth's magnetotail have only been found within such outflow regions [e.g., *Hietala et al.*, 2015]. This schematic view of MH configuration can be investigated and further tested using measurements of plasma (electron) distribution functions.

4. Magnetic Hole Kinetics

We select six examples of deep magnetic holes from Figure 2 and examine their kinetic structures. Figure 5 shows the main parameters within each hole. Taking MH geometry (as shown by Figure 4) into account, we use plasma flows along the x axis to estimate the current density. The electron bulk velocity, v_{ex}, obtained from direct ESA measurements significantly exceeds the ion bulk velocity (v_{ex} reaches 400 km/s,

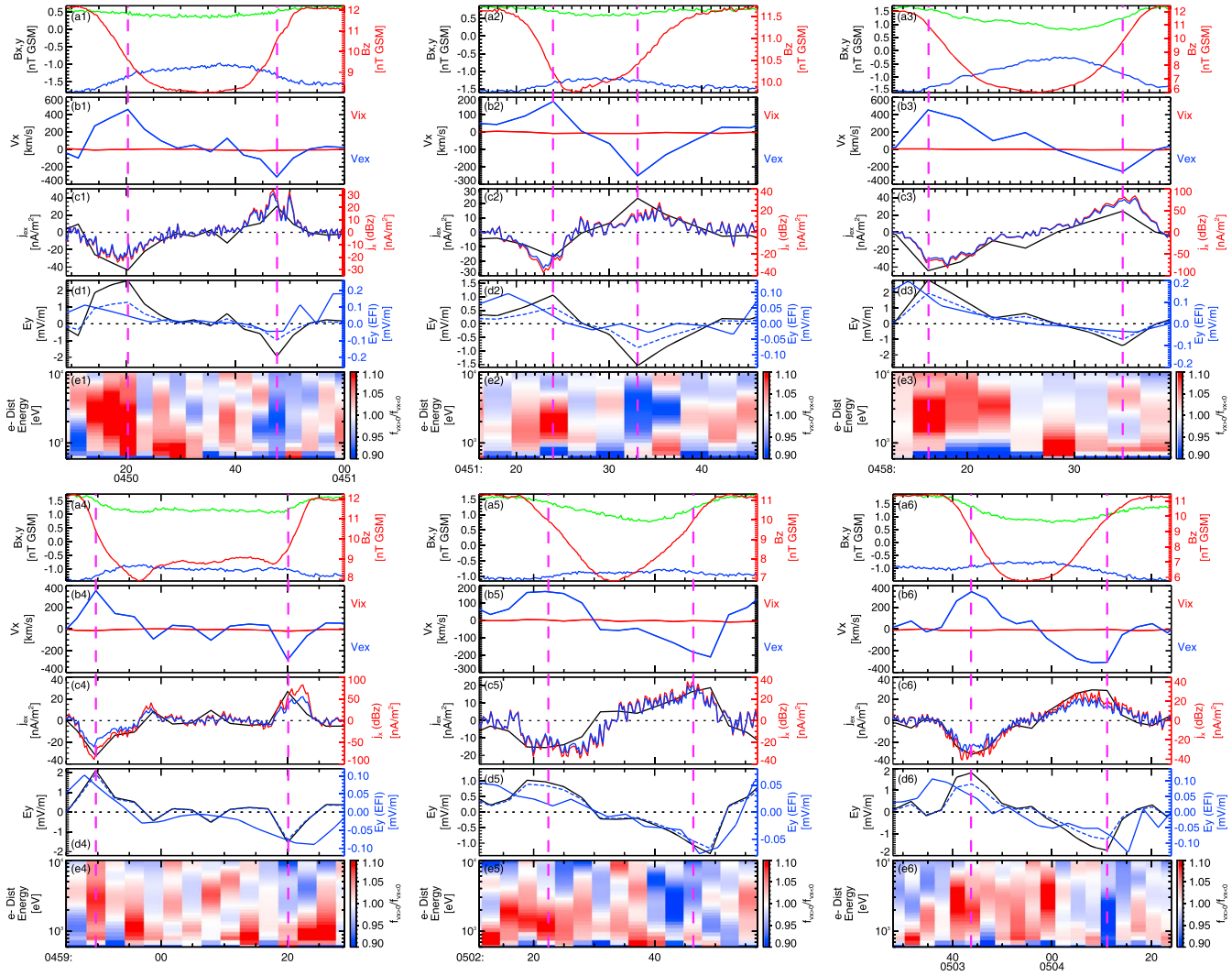

Figure 5. Six examples of deep MHs. For each event: (a) magnetic field B_x (blue), B_y (green), and B_z (red); (b) electron (blue) and ion (red) bulk velocities v_{ex}, v_{ix}; (c) electron current density $j_{ex} = -en_e v_{ex}$ (black), and two current density estimates $j_x = \mu_0(\mathrm{d}B_z/\mathrm{d}t)\langle v_{ion}\rangle^{-1}$ with $\langle v_{ion}\rangle = \langle v_{iy}\rangle$ (red) and $\langle v_{ion}\rangle = \langle\sqrt{v_{ix}^2 + v_{iy}^2}\rangle$ (blue) (velocities are averaged over the hole crossing interval); (d) electric field $E_y = v_{ex}B_z$ calculated for $\delta = \mathrm{d}\ln n_e/\mathrm{d}\ln(T_{e,\perp} + T_{i,\perp}) = 100$ (black, left axis), for $\delta = \mathrm{d}\ln n_e/\mathrm{d}\ln(T_{e,\perp} + T_{i,\perp}) \approx 0.05$ (dashed blue, right axis), and E_y from direct measurements (solid blue, right axis); (e) ratio of the electron phase space density $f_{v_x>0}/f_{v_x<0}$ (sliced at $v_y \approx 0$, $v_z \approx 0$) as a function of energy (see text for details).

comparable with previous observations [*Gershman et al.*, 2016]). Electrons flow in opposite directions at two hole boundaries, generating current density $j_{ex} = -en_e v_{ex}$ that supports the magnetic field gradients. This current density reaches $j_{ex} \sim 50$ nA/m^2. We compare j_{ex} with the current density estimated from the magnetic field gradient, $j_x = -\mu_0^{-1}\mathrm{d}B_z/\mathrm{d}y = -\mu_0(\mathrm{d}B_z/\mathrm{d}t)\langle v_{ion}\rangle^{-1}$, where the hole is assumed to convect with the ion velocity, $\langle v_{ion}\rangle$ is calculated both for y component and for $v_{ion} = \sqrt{v_{ix}^2 + v_{iy}^2}$ and averaged over the interval of the hole crossing (following a similar approach in *Ge et al.* [2011]. Figure 5c show that j_{ex} and j_x profiles are very close to each other. For some cases, there is a factor of < 1.5 for the ratio j_x/j_{ex}, likely caused by underestimation of the very weak ion velocity v_{ion}. Such good agreement of current densities derived using two independent techniques (j_{ex} from direct measurements of the electron distribution function and j_x from the magnetic field measurements) implies a robust estimate of j_{ex}.

Currents of magnetized electrons are generated by diamagnetic and $\mathbf{E} \times \mathbf{B}$ drifts. Therefore, to estimate the electric field responsible for $\mathbf{E} \times \mathbf{B}$ drift, we calculate the difference between the measured v_{ex} and the estimated diamagnetic drift velocity $v_{e,\mathrm{drift}} \approx -(\mathrm{d}p_{e,\perp}/\mathrm{d}y)/en_eB_z$. The latter depends on $\mathrm{d}n_e/\mathrm{d}y$ and $\mathrm{d}(T_{e,\perp} + T_{i,\perp})/\mathrm{d}y$. Both gradients contribute to the pressure balance across MHs: $k_B n_e(T_{e,\perp} + T_{i,\perp}) + B_z^2/2\mu_0 \approx const.$

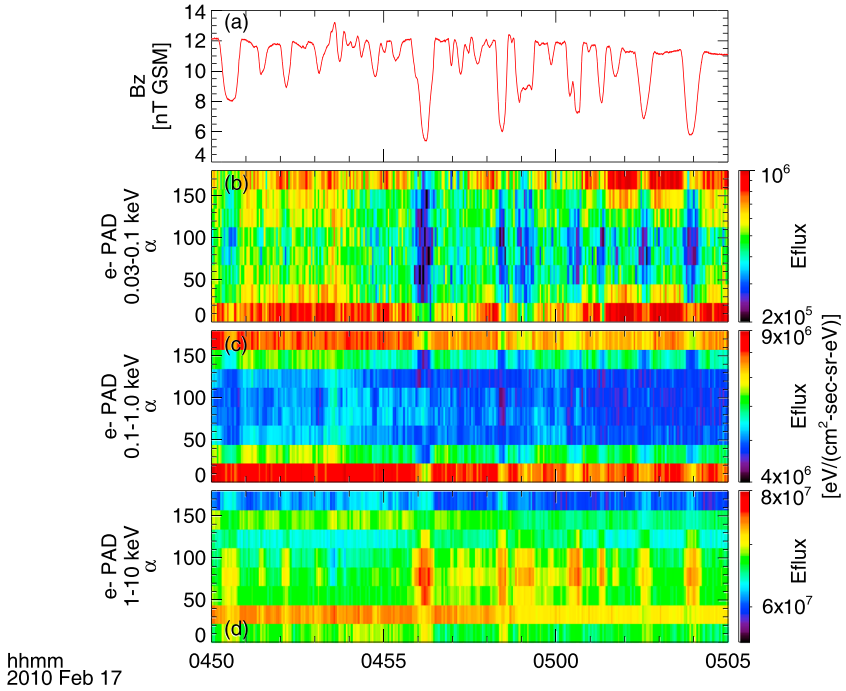

Figure 6. (a) B_z magnetic field and electron pitch-angle distributions in the (b) 0.02–0.1 keV, (c) 0.1 – 1 keV, and (d) 1–10 keV energy ranges. Data are shown for the same interval as in Figure 2.

Uncertainties of n_e and T_e measurements do not allow a direct estimate of $v_{e,drift}$ from the gradients, we thus use the pressure balance condition and introduce the parameter $\delta = \mathrm{d}\ln n_e/\mathrm{d}\ln(T_{e,\perp} + T_{i,\perp})$. When $\delta \ll 1$, the diamagnetic drift is controlled by the electron temperature variation, whereas ions with uniform temperature T_i do not contribute to the pressure balance. When $\delta \gg 1$, the electron diamagnetic drift is controlled by the density variation, whereas the ratio of ion and electron contributions to the pressure balance equals to $T_{i,\perp}/T_{e,\perp}$. Therefore, we estimate the diamagnetic drift for two δ values (0.05 and 100) and calculate the electric field $E_y = (v_{ex} - v_{e,drift})B_z$ required to compensate the remainder of the current through cross-MH potential variation. This estimation is compared with direct electric field measurements.

Figure 5d shows that for large δ the electric field E_y reached a few mV/m, whereas $E_y \sim 0.1$ mV/m for small δ. The latter estimates coincide with the direct electric field measurements (compare solid and dashed blue curves); i.e., the pressure balance and electron diamagnetic drifts are dominated by electron temperature gradients, whereas the density variation is not important.

Gershman et al. [2016] and *Yao et al.* [2017] showed that electron distributions within MHs exhibit significant anisotropies with increased transverse fluxes in the 0.2–4 keV energy range. We checked that the electron population below 500 eV does not contribute to the observed electron bulk velocity v_{ex}, and thus only suprathermal particles are responsible for current generation. To examine the electron velocity distribution in the most anisotropic direction (the current density direction), we consider a slice of the 3-D distribution $f(v_x)$ at $v_y = 0$, $v_z = 0$. Then, we compare the *left* and *right* flanks of this slice: $f_{v_x>0}/f_{v_x<0}$ (as shown in Figure 5e). This ratio is above one for intervals with $v_{ex} > 0$, and below one for intervals with $v_{ex} < 0$. The ratio falls into the [0.9, 1.1] range and maximizes at intermediate energies: $f_{v_x>0}/f_{v_x<0} \sim 1$ (on average) for electrons with energies <1 keV or >6 keV. The asymmetry of left/right flanks of the distribution function results from the diamagnetic and $\sim E_y/B_z$ drifts, which shift the phase space density to negative/positive v_x at two different hole boundaries. Absence of a significant drift in hot (>6 keV) particles can be explained if we consider that the gyroradius (ρ_e) of ~6 keV electrons is ~50 km, comparable with the magnetic field gradient scale (hole boundary scale), ~150 km. Therefore, hot electrons become demagnetized and do not follow $\mathbf{E} \times \mathbf{B}$ drift or gradient drifts constituting the diamagnetic currents at hole boundaries.

The situation is more complicated for lower-energy electrons (<1 keV), which are well magnetized and should follow the $\mathbf{E} \times \mathbf{B}$ drift (but should not contribute to the diamagnetic drift due to their low temperature). For the

observed electron temperature $T_{e\perp} \sim 3$ keV, the lower-energy electron population corresponds to subthermal particles. The isotropization (systematic drifts along x) of this particle population cannot be explained by scattering due to magnetic field gradients. To examine the electron distribution at low energies, we plot pitch angle distributions for three energy ranges: below 100 eV, 0.1–1 keV, and 1–10 keV. As shown by Figure 6, fluxes of low-energy electrons (<1 keV) are predominantly field aligned, whereas thermal and suprathermal electron populations (1–10 keV) are mostly transverse anisotropic. Moreover, within MHs the low-energy electron flux significantly reduces, whereas thermal and suprathermal electron fluxes are enhanced with stronger transverse anisotropy. Therefore, we conclude that the low-energy electron population is dominated by field-aligned flows (of possible ionospheric origin) and the phase space density of transverse ($v_z \sim 0$), cold electrons is rather small. This introduces large uncertainties in $f_{v_x>0}/f_{v_x<0}$ and leads to an isotropic distribution with $f_{v_x>0}/f_{v_x<0} \sim 1$. Does this field-aligned cold electron population contribute to the magnetic hole structure? Integration of the electron distribution up to 0.5 keV produces only ~10% of the total electron density, with almost no contribution to the bulk velocity or the thermal pressure. Thus, we can assume that these cold (at energies <1 keV) electrons do not contribute to MH structure. Similar conclusions, but for energies <0.2 keV, were drawn by *Gershman et al.* [2016].

5. ECH Waves and Field-Aligned Currents Within Magnetic Holes

Magnetic holes significantly modulate ambient electron distributions and the plasma frequency to electron gyrofrequency ratio (ω_{pe}/ω_{ce}) in the system. Figures 7a and 7b show variations of ω_{pe}/ω_{ce} within magnetic holes: ω_{pe}/ω_{ce} increases from the background value ~20 to ~30–40 within the holes. The electron distribution consists of several components and cannot be characterized by the average thermal anisotropy. Therefore, to investigate electron anisotropies at different energies, we show the ratio of electron phase space densities collected for transverse ($f_\perp$) and field-aligned ($f_\parallel$) particles. As demonstrated by Figure 7c, MHs are populated by hot, transversely anisotropic electrons. Electrons within the energy range of [0.3, 3] keV resonate well with ECH waves, and this anisotropic population ($f_\perp/f_\parallel > 1$) can thus significantly influence ECH wave generation/damping. Such significant variations in plasma parameters and the electron distribution should influence generation (and propagation) of electron-scale waves. Generally, increased B_z in a dipolarized plasma sheet makes the loss cone wider and favors electron loss-cone instability, resulting in ECH wave generation [*Karpman et al.*, 1975; *Ashour-Abdalla and Kennel*, 1978; *Ashour-Abdalla et al.*, 1979]. These waves play a crucial role in electron scattering and diffuse aurora formation [e.g., *Ni et al.*, 2012; *Zhang et al.*, 2015; *Ni et al.*, 2016]. Figure 7d shows that observed ECH wave amplitudes (outside MHs) reach 1 mV/m, i.e., we observe rather intense ECH emissions with amplitudes exceeding average values for this region [*Zhang et al.*, 2013]. Interestingly, these ECH emissions are only present outside magnetic holes and almost disappear within them.

To study modulation of ECH emissions by MHs, we use HOTRAY code [*Horne*, 1989] to calculate the linear wave growth rate for electron distributions and plasma/magnetic field parameters outside and inside the holes. We approximate electron distributions inside/outside the hole by a sum of two bi-Maxwellian distributions (see parameters in Table 1) with an imposed loss cone. The loss cone represents a decrease of electron fluxes around the field-aligned (both parallel and antiparallel) direction and is defined by two parameters: the loss cone depth regulates the amplitude of flux depression, and the loss cone width regulates the pitch angle range [*Ashour-Abdalla and Kennel*, 1978]. Both parameters cannot be determined from direct spacecraft measurements, and we use values from a model self-consistently describing the ECH wave intensity in the plasma sheet [*Zhang et al.*, 2013]. We use observed $\omega_{pe}/\omega_{ce} = 50.4$ and 21.6 for the calculation inside and outside MHs. Then we parameterize both ω_{pe}/ω_{ce} and electron distributions by magnetic field magnitude $B \approx B_z$, assuming that parameters inside the holes transit to parameters outside them linearly with B (running from the minimum to maximum value). Using this parametrization, we calculate the ECH growth rate γ for different B values and overplot it along the $B(t)$ profile, as shown in Figure 7e. We use the wave frequency at the peak intensity ($\omega/\omega_{ce} = 1.2$) and a wave normal angle of $\theta = 88°$ derived from ECH waveforms collected by THEMIS around 03:30:26 UT, when burst-mode electric field measurements were available. We see that ECH waves damp within the hole and grow outside the holes. Wave damping within the holes come from the following effect: the significantly increased ω_{pe}/ω_{ce} shifts waves to the long wavelength regime (wavelength is about thermal electron gyroradius ρ_e inside the hole and about a fraction of ρ_e outside the hole), where they are damped by hot electrons. Therefore, modulation of the ECH waves is observed during this event.

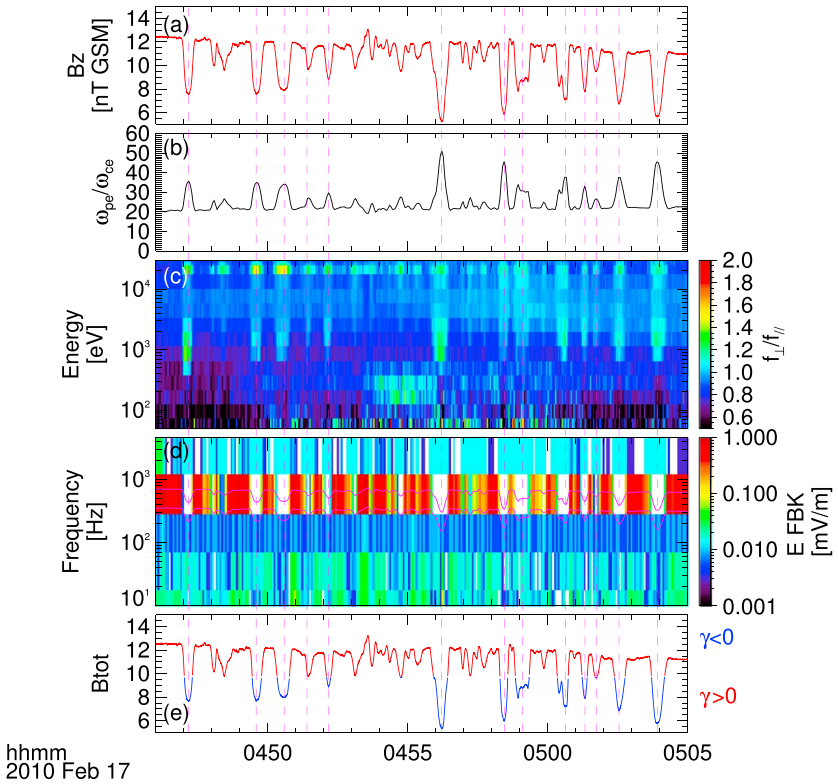

Figure 7. (a) B_z component of magnetic field; (b) ratio of plasma frequency to electron gyrofrequency, ω_{pe}/ω_{ce}; (c) ratio of transverse to parallel electron fluxes plotted versus energy, i.e., for each energy, the color denotes the ratio of electron fluxes measured in transverse direction to those in field-aligned direction; (d) FBK spectrum of the wave electric field (white color indicates frequency bins where the wave intensity is below the detection level of the instrument); (e) magnetic field magnitude color coded by the sign of ECH wave growth rate γ, in red ($\gamma > 0$) or blue ($\gamma < 0$). Maximum/minimum γ values (normalized to ω_{ce}) in our calculation (see text for details) are 0.0439 and −0.0276, respectively. Horizontal lines overplotted in panel (d) are multiples of the equatorial electron gyrofrequency f_{ce} and $2f_{ce}$.

Figure 8 shows that in addition to B_z, magnetic holes are characterized by small B_x variations. Moreover, there is a finite (negative) average B_x across the holes (i.e., we observe them slightly below the neutral plane). Thus, both j_x and $j_z = -\partial B_x/\partial y$ can contribute to the field-aligned current. The full expression for $j_\parallel$ can be written as

$$j_\parallel = j_x\frac{B_x}{B} + j_z\frac{B_z}{B} \approx \mu_0^{-1}\left(\frac{\partial B_z}{\partial y}\frac{B_x}{B} - \frac{\partial B_x}{\partial y}\frac{B_z}{B}\right) \quad (1)$$

Equation (1) describes the field-aligned current flowing along the quasi-1-D MH boundary, i.e., we assume that only gradient along y is significant and neglect the current density component j_y. This assumption is supported by MVA results indicating that the normal direction is along y axis (Figure 3d). The first term within the brackets in equation (1) is negative at the leading MH edge and positive at the trailing MH edge, whereas the second term has opposite polarity, i.e., the two gradients defining the direction of field-aligned currents compete. Figure 8 shows that for some magnetic holes, these two gradients can cancel each other, leading to $j_\parallel \approx 0$. Some magnetic holes have well-resolved field-aligned currents $j_\parallel \leq 5$ nA/m^2, however. Because of the relatively small magnitude

Table 1. Electron Distribution Parameters Inside the Hole (Right Column) and Outside the Hole (Left Column)

Parameter	Outside	Inside
n_1 (cm^{-3})	0.113	0.131
$T_{\perp 1}$ (eV)	310	550
$T_{\parallel 1}$ (eV)	320	540
n_2 (cm^{-3})	0.55	0.58
$T_{\perp 2}$ (eV)	3000	2900
$T_{\parallel 2}$ (eV)	3500	2400
ω_{pe}/ω_{ce}	21.6	50.4

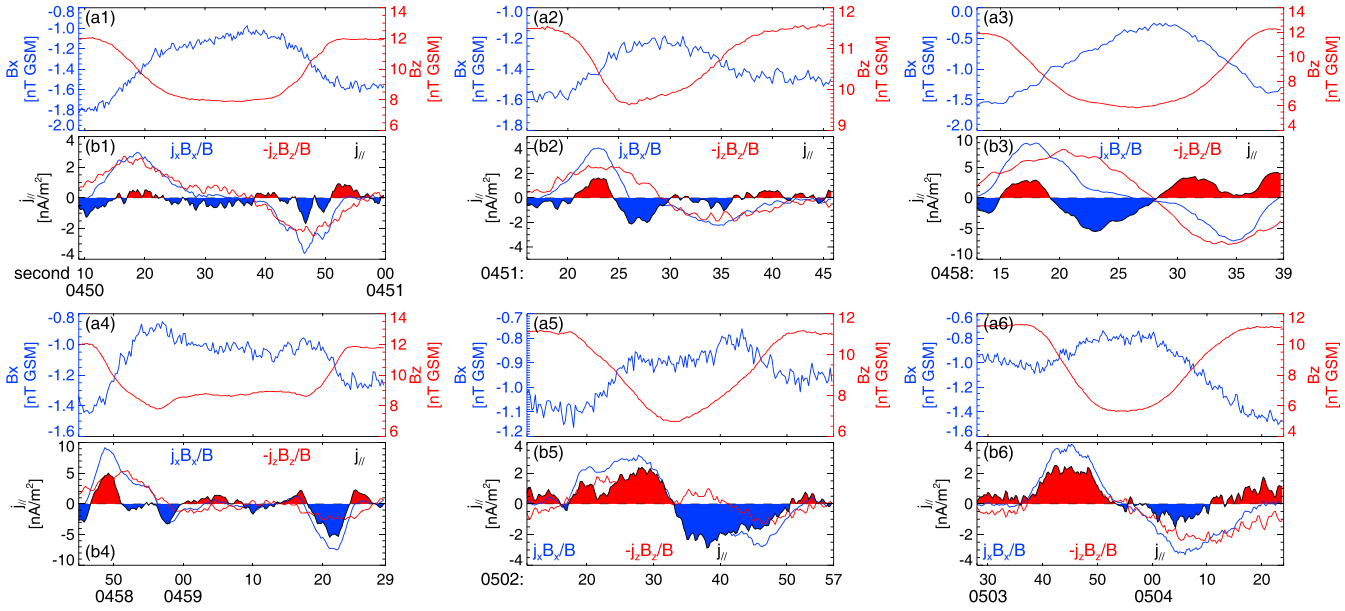

Figure 8. Estimates of current density components contributing to the field-aligned current for the same six MHs shown in Figure 5. For each MH: (a) magnetic field B_x (blue) and B_z (red); (b) j_x, j_z components projected to the background magnetic field direction (shown in blue and red traces), and their summation representing estimates of the field-aligned current density $j_{||}$ (black trace, shaded in red for positive values and blue for negative values).

of $j_{||} \ll j_x$, determination of the field-aligned current density requires accurate calculation of spatial gradients. Such calculations are not always possible because of very slow ion motions used in converting the timescale to spatial scale, which explains why for some MHs, the field-aligned currents are not well resolved. Moreover, as demonstrated by equation (1), calculation of $j_{||}$ requires estimations of both j_x (strong) and j_z (much weaker) currents. The latter component cannot be accurately derived from electron measurements, and thus we cannot compare $j_{||}$ obtained from magnetic field gradients with the directly measured electron field-aligned current.

Although $j_{||}$ seems to be significant (a few nA/m^2), the associated uncertainty level is actually large. While j_x is calculated with an accuracy of ~10–30% (see Figure 5), $j_{||}$ is 1 order of magnitude smaller than j_x. Therefore, $j_{||}$ is within the accuracy range of the current density calculations and further investigations are needed to determine whether these MHs can serve as a local source of field-aligned currents. Spatial scales of observed sub-ion MHs are sufficiently small to justify our assumption of a decoupling of ion/electron motions and the generation of a Hall electric field. In Hall plasma systems, the transverse Hall currents are usually closed by field-aligned currents (such as in magnetic reconnection regions, as demonstrated by e.g., *Yamada et al.* [2010], *Paschmann et al.* [2013, and references therein). To support the MH configuration, field-aligned currents should maximize below and above the magnetotail equatorial ($B_x = 0$) plane, where the system inhomogeneity in the main magnetic field direction results in divergence of the transverse current supported by electron vortexes (e.g., see the current continuity equation in *Vasyliunas* [1970]). Magnetic hole currents support B_z variations without changing its direction (without B_z reversal). Therefore, magnetic field lines in the (y, z) plane (or the (x, z) plane) cannot be closed and should connect to field lines of the magnetotail current sheet. Field-aligned currents along such

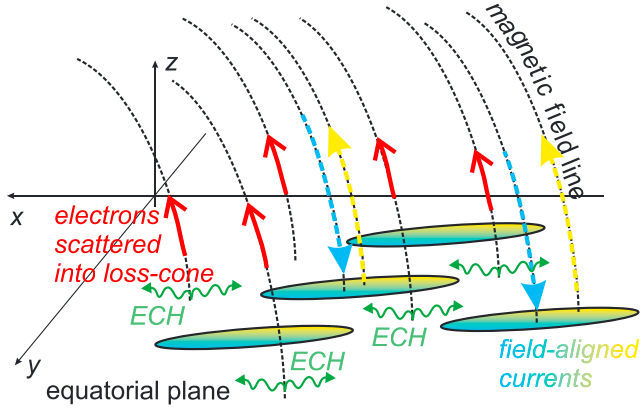

Figure 9. Schematic of MHs connecting the plasma sheet to the ionosphere.

magnetic field lines could be closed in the ionosphere, if not further diverted to transverse currents at some distance from the equatorial plane.

To illustrate results shown in Figures 7 and 8, we plot a schematic view of MHs in Figure 9 connecting the plasma sheet to the ionosphere. The equatorial plane has many sub-ion scale magnetic holes that generate local enhancements of field-aligned currents. Absence of ECH waves within holes results in patchy electron precipitation: scattering into the loss cone is only possible in regions located between MHs. The spatial scales of magnetic holes (~1000 km between closest boundaries) correspond to so-called mesoscale structures in the polar cap, which are usually studied in the context of plasma dynamics (e.g., plasma flows [see *Pritchett et al.*, 2014; *Lyons et al.*, 2016]). We show that modulation of both field-aligned currents and electron precipitation by such mesoscale structures can occur in the quiet dipolarized magnetotail due to electron interactions with MHs.

6. Discussion and Conclusion

The observed magnetic holes are quasi-stationary, captured during quiet geomagnetic conditions after dipolarizations (even though they could have formed originally during dynamic conditions, such as accelerating flows of anisotropic plasma). Therefore, it is reasonable to consider them as self-consistent plasma equilibria embedded into the plasma sheet. At least two theoretical approaches have been used to describe MH configurations and kinetics. The first approach considers a magnetic hole as a plasma equilibrium described by a distribution function from local integrals of motion (the so-called Vlasov approach [see *Schindler*, 2006]). In this approach, a 1-D (plane) magnetic hole can be constructed using distribution functions proposed by *Nicholson* [1963] and *Mottez* [2003]; using the Vlasov approach, a generalized cylindrical geometry was proposed by *Shustov et al.* [2016]. In this approach, the same magnetic field profile can be constructed for significantly different particle distributions (see discussions in *Grad* [1961]). The second approach, which is more physical, includes consideration of MH formation (the system starts with a linearly unstable plasma mode). The growth and saturation of this mode results in formation of quasi-stationary MHs, e.g., such holes can be represented as soliton-like solutions. *Ji et al.* [2014] proposed magnetosonic solitons with Hall electron effects for plane MHs; *Li et al.* [2016] generalized this solution for MHs with cylindrical geometry. An important prediction of this approach is the dependence of MH amplitude and spatial scale on the velocity of MH propagation. *Kuznetsov et al.* [2007] proposed a mirror-mode soliton solution to describe the MH configuration (see more details in *Kuznetsov et al.* [2015]), which depicts the expected relation between MH amplitude and spatial scale. Moreover, the electron vortex within an MH can be described by a model of a potential vortex in hot plasmas [e.g., *Petviashvili and Pokhotelov*, 1992]. Which model is more appropriate to describe observed MHs relies on the comparison between the model and observed kinetics (electron distributions).

The main conclusions of our investigation of magnetic hole kinetics can be summarized as follows:

1. Sub-ion scale magnetic holes are sustained by electron vortexes, in which diamagnetic drifts and electrostatic fields (generated by the ion-electron decoupling) drive electron currents. Although this explanation has already been proposed from observations [*Gershman et al.*, 2016; *Goodrich et al.*, 2016b, 2016a] and simulations [e.g., *Haynes et al.*, 2015], our study has directly demonstrated that the observed electron currents coincide with those derived from magnetic field gradients.
2. Electron currents are generated by electrons of energy range $\sim[T_{e\perp}/3, 2T_{e\perp}]$. Hotter electrons are likely scattered at magnetic field gradients and do not follow diamagnetic and $\mathbf{E}\times\mathbf{B}$ drifts, whereas colder electrons are characterized by a rarified field-aligned population and do not contribute significantly to electron moments (consistent with *Gershman et al.* [2016]).
3. Observed magnetic holes are 3-D structures with two smaller spatial scales in the equatorial plane (transverse to the background magnetic field) and a larger-scale along the background magnetic field. In the equatorial plane, magnetic holes are stretched in the earthward direction. This configuration is not unique (both quasi-1-D and cylindrical magnetic holes were reported by *Balikhin et al.* [2012], *Sundberg et al.* [2015], and *Li et al.* [2016]), but it implies significant spatial anisotropy of the initial plasma configuration where MHs were formed.
4. Within the holes, electron scattering to the loss cone is significantly reduced because of the suppression of ECH waves. The holes, on the other hand, may generate field-aligned currents and thus couple the magnetosphere to the ionosphere on a kinetic (sub-ion gyroradius) scale. Further investigations on the magnetic field gradients and electron kinetics are necessary to verify this conclusion.

Acknowledgments
We thank J. Hohl for her help with editing and F.S. Mozer for important comments about electric field measurements. We acknowledge NASA contract NAS5-02099 for use of data from the THEMIS Mission. We thank J.W. Bonnell and F.S. Mozer for use of EFI data, C.W. Carlson and J.P. McFadden for use of ESA data, D.E. Larson for use of SST data, K.H. Glassmeier, U. Auster, and W. Baumjohann for the use of FGM data provided under the lead of the Technical University of Braunschweig and with financial support through the German Ministry for Economy and Technology and the German Aerospace Center (DLR) under contract 50 OC 0302. All data can be accessed from http://themis.ssl.berkeley.edu/.

References

Angelopoulos, V. (2008), The THEMIS mission, *Space Sci. Rev.*, *141*, 5–34, doi:10.1007/s11214-008-9336-1.
Angelopoulos, V., A. Runov, X. Z. Zhou, D. L. Turner, S. A. Kiehas, S. S. Li, and I. Shinohara (2013), Electromagnetic energy conversion at reconnection fronts, *Science*, *341*, 1478–1482, doi:10.1126/science.1236992.
Artemyev, A. V., W. Baumjohann, A. A. Petrukovich, R. Nakamura, I. Dandouras, and A. Fazakerley (2011), Proton/electron temperature ratio in the magnetotail, *Ann. Geophys.*, *29*, 2253–2257, doi:10.5194/angeo-29-2253-2011.
Artemyev, A. V., A. A. Petrukovich, A. G. Frank, R. Nakamura, and L. M. Zelenyi (2013), Intense current sheets in the magnetotail: Peculiarities of electron physics, *J. Geophys. Res. Space Physics*, *118*, 2789–2799, doi:10.1002/jgra.50297.
Ashour-Abdalla, M., and C. F. Kennel (1978), Nonconvective and convective electron cyclotron harmonic instabilities, *J. Geophys. Res.*, *83*, 1531–1543, doi:10.1029/JA083iA04p01531.
Ashour-Abdalla, M., C. F. Kennel, and W. Livesey (1979), A parametric study of electron multiharmonic instabilities in the magnetosphere, *J. Geophys. Res.*, *84*, 6540–6546, doi:10.1029/JA084iA11p06540.
Auster, H. U., et al. (2008), The THEMIS fluxgate magnetometer, *Space Sci. Rev.*, *141*, 235–264, doi:10.1007/s11214-008-9365-9.
Balikhin, M. A., D. G. Sibeck, A. Runov, and S. N. Walker (2012), Magnetic holes in the vicinity of dipolarization fronts: Mirror or tearing structures?, *J. Geophys. Res.*, *117*, A08229, doi:10.1029/2012JA017552.
Bauer, T. M., W. Baumjohann, R. A. Treumann, N. Sckopke, and H. Lühr (1995), Low-frequency waves in the near-Earth plasma sheet, *J. Geophys. Res.*, *100*, 9605–9618, doi:10.1029/95JA00136.
Bonnell, J. W., F. S. Mozer, G. T. Delory, A. J. Hull, R. E. Ergun, C. M. Cully, V. Angelopoulos, and P. R. Harvey (2008), The Electric Field Instrument (EFI) for THEMIS, *Space Sci. Rev.*, *141*, 303–341, doi:10.1007/s11214-008-9469-2.
Califano, F., P. Hellinger, E. Kuznetsov, T. Passot, P. L. Sulem, and P. M. TráVníčEk (2008), Nonlinear mirror mode dynamics: Simulations and modeling, *J. Geophys. Res.*, *113*, A08219, doi:10.1029/2007JA012898.
Chaston, C. C., J. W. Bonnell, L. Clausen, and V. Angelopoulos (2012), Energy transport by kinetic-scale electromagnetic waves in fast plasma sheet flows, *J. Geophys. Res.*, *117*, A09202, doi:10.1029/2012JA017863.
Cully, C. M., R. E. Ergun, K. Stevens, A. Nammari, and J. Westfall (2008), The THEMIS digital fields board, *Space Sci. Rev.*, *141*, 343–355, doi:10.1007/s11214-008-9417-1.
Deng, X., M. Ashour-Abdalla, M. Zhou, R. Walker, M. El-Alaoui, V. Angelopoulos, R. E. Ergun, and D. Schriver (2010), Wave and particle characteristics of earthward electron injections associated with dipolarization fronts, *J. Geophys. Res.*, *115*, A09225, doi:10.1029/2009JA015107.
Fu, H. S., Y. V. Khotyaintsev, A. Vaivads, M. André, and S. Y. Huang (2012), Electric structure of dipolarization front at sub-proton scale, *Geophys. Res. Lett.*, *39*, L06105, doi:10.1029/2012GL051274.
Ge, Y. S., J. P. McFadden, J. Raeder, V. Angelopoulos, D. Larson, and O. D. Constantinescu (2011), Case studies of mirror-mode structures observed by THEMIS in the near-Earth tail during substorms, *J. Geophys. Res.*, *116*, A01209, doi:10.1029/2010JA015546.
Gershman, D. J., et al. (2016), Electron dynamics in a subproton-gyroscale magnetic hole, *Geophys. Res. Lett.*, *43*, 4112–4118, doi:10.1002/2016GL068545.
Goodrich, K. A., R. E. Ergun, and J. E. Stawarz (2016a), Electric fields associated with small-scale magnetic holes in the plasma sheet: Evidence for electron currents, *Geophys. Res. Lett.*, *43*, 6044–6050, doi:10.1002/2016GL069601.
Goodrich, K. A., et al. (2016b), MMS multipoint electric field observations of small-scale magnetic holes, *Geophys. Res. Lett.*, *43*, 5953–5959, doi:10.1002/2016GL069157.
Grad, H. (1961), Boundary layer between a plasma and a magnetic field, *Phys. Fluids*, *4*, 1366–1375, doi:10.1063/1.1706226.
Haynes, C. T., D. Burgess, E. Camporeale, and T. Sundberg (2015), Electron vortex magnetic holes: A nonlinear coherent plasma structure, *Phys. Plasmas*, *22*(1), 12309, doi:10.1063/1.4906356.
Hietala, H., J. F. Drake, T. D. Phan, J. P. Eastwood, and J. P. McFadden (2015), Ion temperature anisotropy across a magnetotail reconnection jet, *Geophys. Res. Lett.*, *42*, 7239–7247, doi:10.1002/2015GL065168.
Horne, R. B. (1989), Path-integrated growth of electrostatic waves—The generation of terrestrial myriametric radiation, *J. Geophys. Res.*, *94*, 8895–8909, doi:10.1029/JA094iA07p08895.
Hoshino, M., T. Mukai, I. Shinohara, Y. Saito, and S. Kokubun (2000), Slow shock downstream structure in the magnetotail, *J. Geophys. Res.*, *105*, 337–348, doi:10.1029/1999JA900426.
Huang, S. Y., et al. (2012), Observations of turbulence within reconnection jet in the presence of guide field, *Geophys. Res. Lett.*, *39*, L11104, doi:10.1029/2012GL052210.
Hwang, K.-J., M. L. Goldstein, E. Lee, and J. S. Pickett (2011), Cluster observations of multiple dipolarization fronts, *J. Geophys. Res.*, *116*, A00I32, doi:10.1029/2010JA015742.
Ji, X.-F., X.-G. Wang, W.-J. Sun, C.-J. Xiao, Q.-Q. Shi, J. Liu, and Z.-Y. Pu (2014), EMHD theory and observations of electron solitary waves in magnetotail plasmas, *J. Geophys. Res. Space Physics*, *119*, 4281–4289, doi:10.1002/2014JA019924.
Karpman, V. I., I. K. Alekhin, N. D. Borisov, and N. A. Riabova (1975), Electrostatic electron-cyclotron waves in plasma with a loss-cone distribution, *Plasma Phys.*, *17*, 361–372, doi:10.1088/0032-1028/17/5/006.
Khotyaintsev, Y. V., A. Vaivads, M. André, M. Fujimoto, A. Retinò, and C. J. Owen (2010), Observations of slow electron holes at a magnetic reconnection site, *Phys. Rev. Lett.*, *105*(16), 165002, doi:10.1103/PhysRevLett.105.165002.
Kuznetsov, E. A., T. Passot, and P. L. Sulem (2007), Dynamical model for nonlinear mirror modes near threshold, *Phys. Rev. Lett.*, *98*(23), 235003, doi:10.1103/PhysRevLett.98.235003.
Kuznetsov, E. A., T. Passot, V. P. Ruban, and P. L. Sulem (2015), Variational approach for static mirror structures, *Phys. Plasmas*, *22*(4), 42114, doi:10.1063/1.4919027.
Le Contel, O., et al. (2009), Quasi-parallel whistler mode waves observed by THEMIS during near-Earth dipolarizations, *Ann. Geophys.*, *27*, 2259–2275, doi:10.5194/angeo-27-2259-2009.
Li, Z.-Y., W.-J. Sun, X.-G. Wang, Q.-Q. Shi, C.-J. Xiao, Z.-Y. Pu, X.-F. Ji, S.-T. Yao, and S.-Y. Fu (2016), An EMHD soliton model for small-scale magnetic holes in magnetospheric plasmas, *J. Geophys. Res. Space Physics*, *121*, 4180–4190, doi:10.1002/2016JA022424.
Lyons, L. R., Y. Nishimura, and Y. Zou (2016), Unsolved problems: Mesoscale polar cap flow channels' structure, propagation, and effects on space weather disturbances, *J. Geophys. Res. Space Physics*, *121*, 3347–3352, doi:10.1002/2016JA022437.
Lysak, R. L., and Y. Song (2011), Development of parallel electric fields at the plasma sheet boundary layer, *J. Geophys. Res.*, *116*, A00K14, doi:10.1029/2010JA016424.
Matsumoto, H., H. Kojima, T. Miyatake, Y. Omura, M. Okada, I. Nagano, and M. Tsutsui (1994), Electrotastic Solitary Waves (ESW) in the magnetotail: BEN wave forms observed by GEOTAIL, *Geophys. Res. Lett.*, *21*, 2915–2918, doi:10.1029/94GL01284.
McFadden, J. P., C. W. Carlson, D. Larson, M. Ludlam, R. Abiad, B. Elliott, P. Turin, M. Marckwordt, and V. Angelopoulos (2008), The THEMIS ESA plasma instrument and in-flight calibration, *Space Sci. Rev.*, *141*, 277–302, doi:10.1007/s11214-008-9440-2.

Mottez, F. (2003), Exact nonlinear analytic Vlasov-Maxwell tangential equilibria with arbitrary density and temperature profiles, *Phys. Plasmas*, *10*, 2501–2508, doi:10.1063/1.1573639.

Nakamura, R., W. Baumjohann, A. Runov, and Y. Asano (2006), Thin current sheets in the magnetotail observed by cluster, *Space Sci. Rev.*, *122*, 29–38, doi:10.1007/s11214-006-6219-1.

Ni, B., J. Liang, R. M. Thorne, V. Angelopoulos, R. B. Horne, M. Kubyshkina, E. Spanswick, E. F. Donovan, and D. Lummerzheim (2012), Efficient diffuse auroral electron scattering by electrostatic electron cyclotron harmonic waves in the outer magnetosphere: A detailed case study, *J. Geophys. Res.*, *117*, A01218, doi:10.1029/2011JA017095.

Ni, B., et al. (2016), Origins of the Earth's diffuse auroral precipitation, *Space Sci. Rev.*, *200*, 205–259, doi:10.1007/s11214-016-0234-7.

Nicholson, R. (1963), Solution of the vlasov equations for a plasma in an externally uniform magnetic field, *Phys. Fluids*, *6*, 1581–1586.

Norgren, C., A. Vaivads, Y. V. Khotyaintsev, and M. André (2012), Lower hybrid drift waves: Space observations, *Phys. Rev. Lett.*, *109*(5), 55001, doi:10.1103/PhysRevLett.109.055001.

Paschmann, G., M. Øieroset, and T. Phan (2013), In-situ observations of reconnection in space, *Space Sci. Rev.*, *178*, 385–417, doi:10.1007/s11214-012-9957-2.

Petrukovich, A. A., A. V. Artemyev, I. Y. Vasko, R. Nakamura, and L. M. Zelenyi (2015), Current sheets in the Earth magnetotail: Plasma and magnetic field structure with Cluster project observations, *Space Sci. Rev.*, *188*, 311–337, doi:10.1007/s11214-014-0126-7.

Petviashvili, V., and O. Pokhotelov (1992), *Solitary Waves in Plasmas and in the Atmosphere*, Taylor and Francis, Philadelphia, Pa.

Pritchett, P. L., F. V. Coroniti, and Y. Nishimura (2014), The kinetic ballooning/interchange instability as a source of dipolarization fronts and auroral streamers, *J. Geophys. Res. Space Physics*, *119*, 4723–4739, doi:10.1002/2014JA019890.

Roytershteyn, V., H. Karimabadi, and A. Roberts (2015), Generation of magnetic holes in fully kinetic simulations of collisionless turbulence, *Philos. Trans. R. Soc. A*, *373*, 20140151, doi:10.1098/rsta.2014.0151.

Runov, A., V. Angelopoulos, V. A. Sergeev, K. Glassmeier, U. Auster, J. McFadden, D. Larson, and I. Mann (2009a), Global properties of magnetotail current sheet flapping: THEMIS perspectives, *Ann. Geophys.*, *27*, 319–328.

Runov, A., V. Angelopoulos, M. I. Sitnov, V. A. Sergeev, J. Bonnell, J. P. McFadden, D. Larson, K. Glassmeier, and U. Auster (2009b), THEMIS observations of an earthward-propagating dipolarization front, *Geophys. Res. Lett.*, *36*, L14106, doi:10.1029/2009GL038980.

Schindler, K. (2006), *Physics of Space Plasma Activity*, Cambridge Univ. Press, Cambridge, U. K., doi:10.2277/0521858976.

Schindler, K., J. Birn, and M. Hesse (2012), Kinetic model of electric potentials in localized collisionless plasma structures under steady quasi-gyrotropic conditions, *Phys. Plasmas*, *19*(8), 82904, doi:10.1063/1.4747162.

Sergeev, V., et al. (2006), Survey of large-amplitude flapping motions in the midtail current sheet, *Ann. Geophys.*, *24*, 2015–2024.

Sergeev, V., V. Angelopoulos, S. Apatenkov, J. Bonnell, R. Ergun, R. Nakamura, J. McFadden, D. Larson, and A. Runov (2009), Kinetic structure of the sharp injection/dipolarization front in the flow-braking region, *Geophys. Res. Lett.*, *36*, L21105, doi:10.1029/2009GL040658.

Shustov, P. I., A. V. Artemyev, I. Y. Vasko, and E. V. Yushkov (2016), Kinetic models of sub-ion cylindrical magnetic hole, *Phys. Plasmas*, *23*(12), 122903, doi:10.1063/1.4972093.

Sonnerup, B. U. Ö., and L. J. Cahill Jr. (1968), Explorer 12 observations of the magnetopause current layer, *J. Geophys. Res.*, *73*, 1757–1770, doi:10.1029/JA073i005p01757.

Soucek, J., E. Lucek, and I. Dandouras (2008), Properties of magnetosheath mirror modes observed by Cluster and their response to changes in plasma parameters, *J. Geophys. Res.*, *113*, A04203, doi:10.1029/2007JA012649.

Sun, W. J., et al. (2012), Cluster and TC-1 observation of magnetic holes in the plasma sheet, *Ann. Geophys.*, *30*, 583–595, doi:10.5194/angeo-30-583-2012.

Sundberg, T., D. Burgess, and C. T. Haynes (2015), Properties and origin of subproton-scale magnetic holes in the terrestrial plasma sheet, *J. Geophys. Res. Space Physics*, *120*, 2600–2615, doi:10.1002/2014JA020856.

Teh, W.-L., S. Eriksson, B. U. Ö. Sonnerup, R. Ergun, V. Angelopoulos, K.-H. Glassmeier, J. P. McFadden, and J. W. Bonnell (2010), THEMIS observations of a secondary magnetic island within the Hall electromagnetic field region at the magnetopause, *Geophys. Res. Lett.*, *37*, L21102, doi:10.1029/2010GL045056.

Teh, W.-L., R. Nakamura, B. U. Ö. Sonnerup, J. P. Eastwood, M. Volwerk, A. N. Fazakerley, and W. Baumjohann (2011), Evidence of the origin of the Hall magnetic field for reconnection: Hall MHD reconstruction results from Cluster observations, *J. Geophys. Res.*, *116*, A11218, doi:10.1029/2011JA016991.

Tenerani, A., O. L. Contel, F. Califano, P. Robert, D. Fontaine, N. Cornilleau-Wehrlin, and J.-A. Sauvaud (2013), Cluster observations of whistler waves correlated with ion-scale magnetic structures during the 17 August 2003 substorm event, *J. Geophys. Res. Space Physics*, *118*, 6072–6089, doi:10.1002/jgra.50562.

Thorne, R. M., B. Ni, X. Tao, R. B. Horne, and N. P. Meredith (2010), Scattering by chorus waves as the dominant cause of diffuse auroral precipitation, *Nature*, *467*, 943–946, doi:10.1038/nature09467.

Vasyliunas, V. M. (1970), Mathematical models of magnetospheric convection and its coupling to the ionosphere, in *Particles and Field in the Magnetosphere, Astrophysics and Space Science Library*, vol. 17, edited by B. M. McCormack and A. Renzini, pp. 60–71, Springer, Dordrecht, Netherlands, doi:10.1007/978-94-010-3284-1-6.

Vörös, Z. (2011), Magnetic reconnection associated fluctuations in the deep magnetotail: ARTEMIS results, *Nonlinear Processes Geophys.*, *18*, 861–869, doi:10.5194/npg-18-861-2011.

Wang, C., M. Gkioulidou, L. R. Lyons, and V. Angelopoulos (2012), Spatial distributions of the ion to electron temperature ratio in the magnetosheath and plasma sheet, *J. Geophys. Res.*, *117*, A08215, doi:10.1029/2012JA017658.

Wang, R., et al. (2016), Coalescence of magnetic flux ropes in the ion diffusion region of magnetic reconnection, *Nat. Phys.*, *12*, 263–267, doi:10.1038/nphys3578.

Wygant, J. R., et al. (2005), Cluster observations of an intense normal component of the electric field at a thin reconnecting current sheet in the tail and its role in the shock-like acceleration of the ion fluid into the separatrix region, *J. Geophys. Res.*, *110*, A09206, doi:10.1029/2004JA010708.

Yamada, M., R. Kulsrud, and H. Ji (2010), Magnetic reconnection, *Rev. Modern Phys.*, *82*, 603–664, doi:10.1103/RevModPhys.82.603.

Yao, S. T., et al. (2017), Observations of kinetic-size magnetic holes in the magnetosheath, *J. Geophys. Res. Space Physics*, *122*(2), 1990–2000, doi:10.1002/2016JA023858.

Zelenyi, L., A. Artemyev, and A. Petrukovich (2015), Properties of magnetic field fluctuations in the Earth's magnetotail and implications for the general problem of structure formation in hot plasmas, *Space Sci. Rev.*, *188*, 287–310, doi:10.1007/s11214-014-0037-7.

Zhang, T. L., et al. (2005), Double Star/Cluster observation of neutral sheet oscillations on 5 August 2004, *Ann. Geophys.*, *23*, 2909–2914.

Zhang, X., V. Angelopoulos, B. Ni, R. M. Thorne, and R. B. Horne (2013), Quasi-steady, marginally unstable electron cyclotron harmonic wave amplitudes, *J. Geophys. Res. Space Physics*, *118*, 3165–3172, doi:10.1002/jgra.50319.

Zhang, X., V. Angelopoulos, B. Ni, R. M. Thorne, and R. B. Horne (2014), Extent of ECH wave emissions in the Earth's magnetotail, *J. Geophys. Res. Space Physics*, *119*, 5561–5574, doi:10.1002/2014JA019931.

Zhang, X.-J., V. Angelopoulos, B. Ni, and R. M. Thorne (2015), Predominance of ECH wave contribution to diffuse aurora in Earth's outer magnetosphere, *J. Geophys. Res. Space Physics*, *120*, 295–309, doi:10.1002/2014JA020455.